Nature Communications

https://doi.org/10.1038/s41467-026-68338-y

Article in Press

Robust water-activated tissue adhesive patch for arterial/heart wound closure after intervention surgery

Received: 11 May 2025

Accepted: 24 December 2025

Cite this article as: Huang, Y., Zhu, Q., Gu, Y. *et al.* Robust water-activated tissue adhesive patch for arterial/heart wound closure after intervention surgery. *Nat Commun* (2026). https://doi.org/10.1038/s41467-026-68338-y

Yuxuan Huang, Qiuwen Zhu, Yuqing Gu, Rong Wang, Chang Xie, Qianqian Zhu, Qi Jiang, Renjie Liang, Yi Zhang, Youzhi Cai, Yi Hong & Hongwei Ouyang

Robust water-activated tissue adhesive patch for arterial/heart wound closure after intervention surgery

Yuxuan Huang[1,2#], Qiuwen Zhu[1,2#], Yuqing Gu[1,2#], Rong Wang[1,2], Chang Xie[1,2], Qianqian Zhu[3], Qi Jiang[1,2], Renjie Liang[1,2], Yi Zhang[1,2], Youzhi Cai[4]*, Yi Hong[1,2,5]*, Hongwei Ouyang[1,2,5]*

[1] Department of Sports Medicine of the Second Affiliated Hospital, and Liangzhu Laboratory, Zhejiang University School of Medicine, Hangzhou, China.

[2] Dr. Li Dak Sum & Yip Yio Chin Center for Stem Cells and Regenerative Medicine, Zhejiang University School of Medicine, Hangzhou, China.

[3] Department of Vascular Surgery, The First Affiliated Hospital, School of Medicine, Zhejiang University, Hangzhou, China.

[4] Department of Orthopedics, The First Affiliated Hospital, Zhejiang University School of Medicine, Hangzhou, China.

[5] China Orthopedic Regenerative Medicine Group (CORMed), Hangzhou, China.

# These authors contributed equally

* These authors jointly supervised this work

E-mail address: hwoy@zju.edu.cn, yihong@zju.edu.cn, caiyouzhi@zju.edu.cn

Abstract

Sealing of puncture points subsequent to interventional surgeries is a vital requirement for all interventional operations. Currently, large-diameter sheaths and transapical punctures present a significant challenge for wound closure, with a high probability of failure. In this study, we've developed a water-activated tissue adhesive patch (WAP) designed for quick and strong adhesion to blood vessel and heart tissue surfaces after surgery. This patch consists of a polyethylene glycol (PEG) derivative coating and a gelatin sponge. Upon contact with a vascular or cardiac wound, the PEG derivative coating quickly absorbs water, dissolves, undergoes rapid crosslinking, and adheres to the tissue surface. This patch can endure a burst pressure more than 300 mmHg and exhibits good biosafety, thereby ensuring effective wound closure and healing. Animal studies have demonstrated that the patch effectively closes wounds and rapidly achieves hemostasis through simple adhesion. This has been exemplified in male porcine models, including heart stab wounds, femoral artery punctures using a 14 Fr sheath, and abdominal aorta punctures with a 20 Fr sheath. Follow-up evaluations indicate favorable postoperative wound healing. When paired with a suitable delivery device, the WAP stands as a potent candidate for the next generation of vascular and transapical closure device.

Introduction

Interventional surgery has emerged as a vital therapeutic intervention for cardiovascular and neurological disorders, mostly performed via radial and femoral artery punctures[1]. Currently, vascular closure devices commonly used in clinical practice, such as ProGlide®, close the vessels through suturing. However, these devices exhibit a high rate of failure when employed for large-diameter sheath punctures[2,3]. Though the ProGlide® device is approved for arterial punctures of 5–21 Fr sheath size, with the maximum diameter being 26 Fr, sheath sizes exceeding 19 Fr have been significantly correlated with device failure, necessitating conversion to a femoral cutdown in the event of a primary failure of the percutaneous endovascular approach[4]. Meanwhile, the use of the ProGlide® and other suture-based vascular closure devices is not considered for patients with vascular conditions such as calcification and angiosclerosis[5,6].

In addition to vascular interventions, transapical puncture interventions are also extensively used in clinical practice due to several benefits, including direct access to the heart, avoidance of vascular complications, compatibility with patients with peripheral artery disease, and less bleeding risk[7]. Due to the constant heartbeat and high pressure, a small incision of about 10 mm is typically made in the heart during the procedure, and the puncture hole at the heart's apex is sealed by suturing[8]. Currently, all devices used for transapical closure are suture-based. Among these, the Apica ASC™ device received a CE mark in 2013[9], and the Permaseal™ device obtained FDA approval in 2016. Other devices are still in the clinical trial stage[10].

Currently, there exist several non-suturing vascular closure devices in clinical application, including the Manta and Angio-Seal. These devices operate by gripping the vascular wall internally and externally with materials, forming a sandwich-like configuration to seal the injury. However, the theoretical risk of limb ischemia deriving from thrombosis is elevated with the utilization of intraluminal vascular closure devices[11,12], and instances of occlusion or thrombosis subsequent to the deployment of these vascular closure devices have been documented[13-16]. An alternative category of non-suturing closure devices functions by positioning plug-like materials exterior to the vessel. The puncture site is sealed by the pressure generated from the swelling of these materials as they absorb blood. Nevertheless, these devices are limited to puncture sheaths smaller than 12 Fr[17,18]. For larger puncture wounds, due to the high pressure, it is challenging to maintain closure.

An ideal closure device should be applicable to various healthy and diseased tissues and should avoid retaining materials in the blood vessel to prevent the risk of thrombosis. The tissue adhesive patch is a promising material for closure devices and has been extensively studied[19,20]. Although previous studies have developed hydrogel patches capable of adhering to wet tissues[21-24], their effectiveness in controlling severe bleeding, such as from transapical punctures sites or arterial intervention sites, remains limited. To achieve wound closure in bleeding environments after interventional surgery, adhesion under blood is especially critical. Large amounts of water in blood can interfere with the reaction between adhesive groups and tissues, potentially preventing a solid closure[25]. Various studies have proposed different water-displacing strategies. Some use hydrophobic interactions to repel

water, allowing for increased contact between the adhesive and tissue surfaces[26]. Others eliminate water from the tissue surface through ion-liquid and aqueous solution exchanges[27]. Some suggest protecting active ingredients within stabilizers, using the stabilizer's underwater diffusion to expose the effective components[28,29]. However, due to challenges like adhesion speed, material safety, and material form, there's currently no tissue adhesive patch available for vascular or transapical closure after intervention puncture surgery.

To achieve this purpose, we herein explored a water-activated tissue adhesive patch (WAP) that can quickly and strongly adhere to the surface of blood vessels and the heart after intervention surgery to achieve wound closure and prevent blood loss. WAP not only exhibits strong wet-tissue adhesion but also functions effectively in scenarios of massive bleeding following transapical puncture and arterial intervention. WAP is composed of a polyethylene glycol (PEG) derivative coating and a gelatin sponge composite (Figure 1 and Supplementary Figure 1). In this system, water not only does not interfere with adhesion, but becomes a prerequisite to trigger adhesion. As shown in Figure 1, when the patch comes into contact with a tissue surface covered with a large amount of blood, the PEG derivative coating dissolves quickly and forms a high-viscosity fluid, which greatly absorbs water and temporarily pushes away the blood on the wound surface, allowing the adhesive groups and tissue surface to fully contact, thereby reducing the impact of blood on tissue adhesion. At the same time, the dissolution of the coating triggers rapid in-situ cross-linking of PEG, forming an interpenetrating network between the polymer and the tissue, which contributes to rapid and high-strength tissue adhesion. Finally, the hydrogel patch formed *in situ* achieves wound closure and promotes subsequent tissue repair. The burst pressure of WAP on aorta reaches 316 mmHg. Additionally, WAP shows excellent biocompatibility and can degrade within the body. Using severe bleeding models, including rabbit femoral artery massive bleeding, porcine heart stab injury massive bleeding, porcine abdominal aorta puncture massive bleeding, and porcine femoral artery puncture massive bleeding, we've demonstrated WAP's superior ability of wound closure. When used with the right accessories, WAP could potentially be employed in the construction of a next generation vascular and transapical closure device.

Results and discussion

Fabrication of WAP

As shown in Figure 1, the adhesive layer of WAP is composed of two key elements. The primary component consists of PEG derivatives, specifically acrylate-modified PEG (PEGAA), acting as the foundational structure. Upon exposure to blood, these polymers rapidly dissolve, forming a viscous solution that displaces blood by leveraging a viscosity differential. The second component is a redox system of two small molecules designed to initiate free radical polymerization. Potassium persulfate (KPS) is used as the oxidant while ferrous ion (Fe^{2+}) is used as the reductant. Following water absorption, these small molecules dissolve quickly along with the PEG matrix, prompting PEG crosslinking and facilitating a shift from solution to solid-state hydrogel. PEG derivatives have been extensively utilized in the development of medical adhesives, such as the FDA-approved sealant Coseal, a two-component system comprising thiol-modified PEG and succinimidyl-modified PEG solutions[30]. However, such solution-based adhesives are prone to being washed away, limiting their efficacy in conditions involving significant bleeding. In addition to Coseal, Hemopatch represents a notable sealant composed of a collagen matrix coated with succinimidyl-modified PEG. However, its low burst pressure (< 40 mmHg) limits its efficacy in managing arterial bleeding[31,32]. To the best of our knowledge, PEG-based adhesive capable of addressing the challenges posed by massive hemorrhage have not been explored. Additionally, the adhesive potential of acrylate-modified PEG remains an underexamined area of research.

By the material design illustrated in Figure 1, we propose that two separate mechanisms synergistically contribute to robust adhesion of WAP. The first mechanism involves a physical interlock between the adhesive matrix and the tissue extracellular matrix (ECM)[33]. Upon dissolution of PEG, its molecules randomly diffuse and penetrate the tissue surface before achieving complete crosslinking, thereby forming physical interactions with the ECM. While such a strategy has been previously employed in tissue adhesives, it typically relies on external cues for activation[34,35]. In contrast, our design achieves this effect using only water from the physiological environment. As shown in Supplementary Figure 2, there is a clear overlap at both the adhesive layer-sponge interface and the adhesive layer-tissue interface. This finding confirms that during water-triggered adhesion, molecular chains in the hydrogel layer interpenetrate both the gelatin sponge and the ECM, establishing a robust and stable connection.

The second mechanism is likely related to thiol-ene click chemistry, wherein acrylate groups react with thiol groups present in proteins within the extracellular matrix (ECM). While such reactions have been explored for tissue adhesives, existing studies report reaction times ranging from minutes to hours[36,37], making them unsuitable for hemostasis. Typically, thermal, oxidation–reduction, or photochemical process is required to initiate the free-radical-based thiol-ene chemistry[38]. The design of WAP incorporates redox-catalyzed crosslinking of PEGAA, generating an abundance of free radicals at the double bonds. These radicals, in turn, could react with thiol groups on the tissue, forming stable covalent interactions and further strengthening the

adhesion. Through the water-activated strategy, the reaction of thiol-ene chemistry is hypothesized to be faster, making it a feasible mechanism for urgent hemostatic applications.

In addition to these two dominant mechanisms, other non-covalent interactions may also play auxiliary roles during the initial adhesion process. For instance, weak hydrogen bonding or dipolar interactions between PEG derivatives and polar groups on the tissue surface could transiently enhance molecular interpenetration and network formation. While such secondary interactions may modestly assist in early-stage adhesion, the overall adhesion strength of WAP primarily arises from the physical interlock and redox-initiated thiol–ene covalent bonding.

Optimization of WAP formula

The occurrence of two distinct phase transitions during the adhesion process suggests that the relative component ratios are critical in determining whether an interpenetrating hydrogel network is formed within the tissue's extracellular matrix (ECM), thereby ensuring reliable adhesion. We optimized the formula of WAP by performing adhesion strength assessments. To facilitate testing, the adhesive layer was cryo-milled to yield an adhesive powder, which was used for further testing on adhesive performance. The primary macromolecule contributing to the formation of the hydrogel network is PEGAA. We hypothesize that its molecular weight and branching degree significantly influence intermolecular interactions[39], which in turn determine the resultant adhesive properties post-gelation. Initially, we employed 20 kDa 4-arm PEGAA as the sole PEG derivative; however, effective adhesion was not achieved. We speculate that this was due to the slow dissolution rate of the compound, which was incompatible with the oxidation-reduction crosslinking rate. Upon switching to 1,000 Da linear PEGAA (PEGDA), which dissolves more rapidly, we observed some adhesion. However, the resulting PEGDA-based hydrogel exhibited brittleness likely due to the higher ratio of short network units[40], reduced cohesion strength, and consequently lower adhesion performance. Additionally, the shorter molecular chains of PEGDA hindered the mechanical interlocking between the hydrogel and the ECM. To optimize adhesion strength, we combined PEGDA with 4-arm PEGAA. Compared to the control group, which was solely composed of 1,000 Da PEGDA, hydrogels containing 4-arm PEGAA demonstrated significantly enhanced tissue adhesion. As the molecular weight of 4-arm PEGAA increased from 5 kDa to 20 kDa, the hydrogel's adhesion strength improved from 41.8 kPa to 105.9 kPa (Figure 2a and Supplementary Figure 3). By combining two PEG derivatives with different molecular weights and branching degrees, we hypothesize that the rapidly dissolving PEGDA generates free radicals in the oxidation-reduction system, which facilitates the crosslinking of 4-arm PEGAA and promotes the formation of stable covalent bonds with the ECM, thereby enhancing the overall adhesive performance

The structural integrity of the resulting hydrogel is another crucial factor influencing the sealing capability of the adhesive layer. The integrity largely depends on the gelation rate during the second phase transition in the "solid-liquid-solid" dual-phase process, regulated by the ratio of the redox system to the double bonds on PEG molecules. We assessed the gelation rate in the solution phase, as indicated in supplementary table, by

systematically adjusting the redox system ratio while maintaining a fixed PEG terminal concentration, identifying several conditions with gelation times under 10 seconds. As the proportion of the redox system decreased, the gelation time gradually increased. When the redox system-to-double bond ratio was raised from 1:15 to 1:10, we observed a significant increase in gelation time of approximately 2 seconds. Additionally, using representative ratios that achieved gelation times within 10 seconds, we prepared adhesive powders and conducted adhesion test on porcine muscle samples immersed under blood to evaluate the integrity of the formed hydrogel. Specifically, adhesive powder was compression-molded into 10-mm diameter samples. After crosslinking under blood and adhering to tissue, the ratio of the formed hydrogel area to its initial area was measured and defined as the gelation completion index, or integrity. Results showed that adhesive powders undergoing two phase transitions demonstrated marked variations in hydrogel integrity (Figure 2b-c). The system with a solution-based gelation time below 3 seconds (AA: Fe^{2+}: KPS = 10:1:1) achieved the highest hydrogel integrity, reaching 96.9%, and was thus selected for further applications. As the redox system ratio was reduced, hydrogel integrity decreased from 43.4% (AA: Fe^{2+}: KPS = 20:1:1) to as low as 2.2% (AA: Fe^{2+}: KPS = 100:1:1). Given that the gelation time of adhesive powders immersed in blood may deviate from that observed in solution, a comprehensive evaluation of results from both conditions is required to identify the optimal ratio.

Further, we optimized the ratio of the two polymers that form the hydrogel matrix: PEGDA with a molecular weight of 1000 and 4-arm-PEGAA with a molecular weight of 20,000. We assessed the adhesive performance of adhesive powder prepared with various PEG ratios on porcine muscle samples, using PBS and fresh porcine blood as interface liquids. When water was the interface liquid (Figure 2d and Supplementary Figure 4), the shear strength of the self-adhesive hydrogel increased as the PEGDA ratio rose, likely due to the faster dissolution rate of the solid powder, enabling more rapid water displacement. When blood was used as the interface liquid (Figure 2e and Supplementary Figure 5), the shear strength of the hydrogel similarly exhibited an upward trend with increasing PEGDA ratios, though this trend was less consistent than with water alone, likely due to the heterogeneous protein composition in blood. Based on these findings, we selected PEGDA: 4-arm-PEGAA = 3:1 as the final formulation, due to its optimal performance during under blood adhesive tests.

***In vitro* Adhesive performance of WAP**

To evaluate the adhesive efficacy of the WAP layer on various tissues, different tissues were bonded with the adhesive powder, with fresh porcine blood served as the interface liquid. The adhesive performance was evaluated via lap shear testing. The adhesive powder exhibited substantial adhesive property across diverse tissue types (Figure 2f and Supplementary Figure 6), achieving a peak shear strength of approximately 47.1±6.3 kPa in gastric tissue. Even in lung tissue, where the adhesive was the weakest, the measured shear strength was approximately 16.2±4.9 kPa, indicating the potential of the adhesive for hemostatic application in various tissues. Under lap shear testing conditions, the adhesive performance of WAP was evaluated against several commercial counterparts, including the PEG-based sealant CoSeal, fibrin sealants, and cyanoacrylate sealants. The results

demonstrated that WAP consistently outperformed these products in adhesive strength (Figure 2g). When comparing the adhesive powder's interfacial toughness (89.4±7.7 $J \cdot m^{-2}$) with that of commercially available adhesives, it markedly outperformed these adhesives as reported in previous literature [33,41-51], including the gelatin-based hemostatic agent Surgiflo, fibrin sealants, the albumin-based adhesive BioGlue, the PEG-based sealant CoSeal, and the cyanoacrylate adhesive, thus underscoring its superior adhesion to moist tissue surfaces (Supplementary Figure 7). It should be noted that in some references, the adhesives were merely tested on wet tissue without blood, further indicating that these commercially available products are hard to use in massive bleeding occasions.

Furthermore, we tested the sealing capacity of adhesive powder by adhering to an incision in a small intestine casing and measuring the burst pressure of the resulting hydrogel (Figure 2h). The adhesive powder alone yielded a burst pressure of 155.17 mmHg. When integrated with a gelatin sponge to create the WAP composite, the burst pressure rose to 227.52 mmHg, indicating that the combination of gelatin sponge significantly improved the hydrogel patch's mechanical robustness (Figure 2h). Both the adhesive layer and the WAP composite exhibited burst pressures exceeding those of commercially available fibrin glue (~63 mmHg)[51], demonstrating resilience to normal physiological blood pressures (90–120 mmHg)[51]. While the hydrogel formed by the adhesive layer alone may present a risk in hemostasis for individuals with hypertension (>140 mmHg), the WAP composite's enhanced structure, fortified by the gelatin sponge, effectively withstood pressures characteristic of severe hypertension (~180 mmHg).

Blood vessels reside within various dynamic soft tissues, with organ injuries frequently accompanied by hemorrhaging. To evaluate WAP's sealing capabilities for different organ injuries, we conducted a series of validation experiments using ex vivo models. An aorta was connected to a pump to simulate blood flow, and upon arterial damage, significant fluid leakage from the vessel replicated the conditions of major hemorrhage. By simply pressing WAP onto the defect for 15 seconds, the arterial rupture was entirely sealed, restoring the vessel to full pressurization. Pressure measurements indicated that the WAP-sealed aorta could endure a maximum pressure of 316 mmHg, far exceeding typical hypertensive blood pressures (~180 mmHg). Upon removal of the gelatin sponge backing from the WAP, a clear hydrogel layer was observed to be securely adhered to the aortic surface (Supplementary Figure 8a). In addition to its vascular sealing abilities, WAP demonstrates versatile sealing potential for injuries in other soft tissues. WAP effectively seals air leaks in traumatized lung lobes, facilitating lung reinflation (Supplementary Figure 8b), and similarly addresses fluid leaks in injured stomach tissue (Supplementary Figure 8c). Consistent with its vascular performance, WAP forms a cohesive hydrogel layer that securely adheres to moist tissue surfaces. These results suggest that WAP adapts well to various dynamic, moist tissue environments, establishing strong tissue adhesion and holding significant promise for the effective sealing of diverse types of tissue injuries.

Biocompatibility of WAP

For in vivo wound closure, WAP transitions rapidly upon blood exposure from a composite patch to a hydrogel, which showed extended retention within the body. In light of this, the in vitro biocompatibility evaluation involved pre-gelling WAP with culture medium or PBS before further cytotoxicity test. Supplementary Figure 9 presents the cell viability of L929 cells cultured in pre-gelled WAP extract and standard medium over 1, 3, and 5 days. In comparison to the control group where L929 was cultured with standard medium, L929 cells treated with the WAP extract demonstrated viability rates exceeding 90%, indicating no inhibition of cell proliferation. These findings confirm that the extract from the gelled WAP does not exhibit cytotoxic effects in cell contact assays.

The degradation profile of WAP in vivo was evaluated using subcutaneous implantation in rats (Figure 3a-b). At 7 days, a few capillaries were observed around the gel, with well-defined boundaries between the implant and surrounding tissue, and no notable changes in gel mass relative to its initial state. By day 14, the implant had become a rounded sphere, maintaining clear boundary demarcation, and presenting a smooth tissue interface. The gel mass had increased relative to its original implanted state. These gross morphological and mass analyses suggest that by day 14, the hydrogel likely absorbed interstitial fluid from the surrounding tissue, achieving saturation and consequent swelling. Notably, this swelling did not cause tissue compression or edema. By day 28, the previously spherical gel had begun to flatten, with a substantial reduction in mass, marking the onset of degradation. By day 56, the gel had collapsed further, and visible capillary ingrowth was observed, with gel mass reduced to approximately 76% of the day 14 measurement. By day 84, the gel's structure was notably degraded, the encapsulating tissue no longer exhibited a vesicular form, and the gel had lost its regular disc shape, suggesting significant internal degradation. The gel mass at day 84 was reduced to 60% of its day 14 mass. To verify that the initial mass increase after implantation was due to hydrogel swelling, we monitored the weight change of WAP in simulated body fluid over 1–28 days in vitro (Supplementary Figure 10). The results showed more than a threefold swelling within the first three days, followed by a gradual mass decrease from day 7, indicating the onset of degradation. Compared with in vivo implantation, in vitro samples exhibited greater swelling due to full exposure to fluid and slower degradation owing to the absence of enzymes and proteins. The subcutaneous implantation results demonstrate that the WAP remains biocompatible over extended durations in *vivo*, without inducing severe tissue rejection responses such as necrosis or edema. The implant exhibits gradual degradation over time, reaching an approximate 60% degradation by 84 days post-implantation. As vascularization progresses, the degradation rate is anticipated to accelerate. Extrapolating from the observed 84-day degradation rate, we suspect that the implant will completely degrade within approximately nine months.

To further evaluate the biocompatibility of the WAP, we conducted histological analysis on rat subcutaneous tissue samples at different time points following material implantation. Typically, foreign materials implanted in the body prompt the formation of a distinct fibrous capsule around the implant, aligned parallel to its surface. This capsule predominantly comprises flattened fibroblasts and dense collagen fibers, with infiltration by inflammatory cells. The thickness of this capsule serves as a critical indicator of biocompatibility. As shown in

Figure 3c, a pronounced fibrous capsule, approximately 20–50 μm thick, was present at the hydrogel-tissue interface by one-week post-implantation (Day 7). At two weeks (Day 14), the capsule's thickness increased to approximately 50–100 μm, likely due to hydrogel swelling from water absorption, as corroborated by gross morphological analysis (Figure 3a). By four weeks (Day 28), the capsule's thickness had substantially decreased to less than 30 μm, with portions nearly disappearing. By eight and twelve weeks (Days 56 and 84), the fibrous capsule had fully dissolved, aligning with the accelerated hydrogel degradation observed macroscopically. The absence of this capsule promotes direct tissue-hydrogel interaction, further accelerating hydrogel degradation. These results strongly suggest that the WAP exhibits excellent tissue compatibility and is well-suited for extended in vivo applications.

***In vivo* hemostatic performance and potential application of WAP**

Studies indicate that severe hemorrhage can quickly lead to shock that threatens life, while timely hemostasis may provide a few hours of rescue time[52]. However, under conditions of extreme hemorrhage—such as arterial bleeding caused by gunshots or car accidents—identifying the exact bleeding spot is challenging, making hemostasis exceedingly difficult. Consequently, the ability to achieve hemostasis without pinpointing a bleeding source is critically valuable. To evaluate the hemostatic efficacy of WAP, we simulated a severe femoral artery hemorrhage in a rabbit model. We transected the femoral artery along with surrounding muscle tissue using a scalpel without directly exposing the vessel, resulting in extensive hemorrhage that obscured the arterial ends. WAP was applied to the muscle surface with 20 seconds of firm pressure, which effectively stopped the bleeding (Supplementary Figure 11a and Supplementary movie 1). In contrast, in the control group treated with a gelatin sponge lacking an adhesive layer, hemorrhage persisted despite 30 seconds of pressure, and bleeding remained uncontrolled even with continuous pressure for over a minute, (Supplementary Figure 11b and Supplementary movie 2). Additionally, we compressed the femoral artery wound with Surgicel, a hemostatic material commonly used in clinical practice (Supplementary Figure 11c and Supplementary movie 3). Results showed that Surgicel also failed to achieve hemostasis. These findings indicate that in cases of severe femoral artery hemorrhage, WAP can rapidly seal the bleeding region via its strong tissue adhesion, achieving effective hemostasis even in the absence of a discernible bleeding site, thus potentially prolonging the critical rescue window.

The heart is prone to rapid hemorrhagic shock and fatality following traumatic injury due to the swift and significant loss of blood. Moreover, achieving effective hemostasis after transapical procedures remains an unmet clinical challenge. To further substantiate WAP's hemostatic efficacy in vivo and verify its potential as a closure device, we conducted a stab wound hemostasis experiment on a porcine heart model. As illustrated in Figure 4a, a scalpel was used to puncture the right ventricle, which led to a considerable expulsion of blood from the wound with each heartbeat. In the absence of other emergency interventions, WAP was immediately applied to the wound with sustained pressure for 30 seconds on the actively beating heart, successfully stopping the hemorrhage entirely (Supplementary movie 4). During the experiment, Blood loss was estimated by gauging the

weight increment of standard surgical gauze used to absorb bleeding during the procedure. In this setting, the gauze weight increased by approximately 30–50 mL per sample when using WAP. Considering the estimated blood volume of adult pigs (65–70 mL/kg)[53], and in light of the generally accepted criterion that blood loss of less than 10% of total blood volume is classified as mild hemorrhage[54], the observed bleeding volume after WAP application was relatively minor. Importantly, even in this large-bleed model, no evidence of hypovolemic shock or mortality was observed. Therefore, WAP can endure the elevated ejection pressures typical of cardiac bleeding from puncture injuries, achieving swift and complete occlusion of the bleeding site.

To evaluate long-term cardiac repair, electrocardiography (ECG) and echocardiography were continuously monitored from days 1 to 28 following hemostasis in the porcine model (n=4). In addition, heart rate, plasma aspartate aminotransferase (AST), lactate dehydrogenase (LDH), creatine kinase (CK), and CK-MB levels were measured. Postoperatively, heart rate showed a transient decrease, likely due to anesthesia and surgical stress, but returned to baseline within 7–14 days (Figure 4b and Supplementary Figure 12a). Serum AST, LDH, and CK levels were elevated immediately after surgery, reflecting cardiac injury, and similarly returned to baseline within 7–14 days (Supplementary Figure 12b-d). Importantly, CK-MB levels did not show a significant increase, indicating the absence of myocardial infarction or heart failure (Supplementary Figure 12e). Echocardiographic analysis revealed an increase in left ventricular volume (LVIDd) and end-diastolic volume (EDV), suggesting compensatory dilation. However, ejection fraction (EF) remained stable throughout the 28-day follow-up, with an associated increase in stroke volume (SV), indicating preserved cardiac function without heart failure or functional impairment (Figure 4c, Supplementary Figure 13 and Supplementary movies 5-6). Histological examination at day 28 demonstrated complete closure of the injury site (Figure 4d). No significant inflammatory response was observed around residual material (Figure 4e), and myocardial architecture at the injury site closely resembled that of normal tissue (Figure 4f). Collectively, these findings indicate that the material provides effective hemostasis after transapical puncture and exhibits favorable biocompatibility, supporting its potential as a safe and functional cardiac repair strategy.

Interventional surgery involves vascular access procedures in which catheters or other devices are inserted into blood vessels to facilitate intravascular diagnostics or treatments. A 14F sheath, classified as a large-diameter sheath, is frequently utilized in complex interventions for the introduction of sizable or rigid instruments[55], such as in transcatheter aortic valve replacement (TAVR), thoracic endovascular aortic repair (TEVAR), and endovascular aneurysm repair (EVAR). Hemostasis following the deployment of a 14F sheath is a critical step, as delayed or improper hemostasis can lead to severe hemorrhagic complications, including oozing, active bleeding, hematoma, pseudoaneurysm, or arteriovenous fistula formation[56]. Hemostatic techniques after a 14F sheath intervention include manual compression, mechanical compression[57], and the use of vascular closure devices[12]. Both manual and mechanical compressions involve sustained pressure on the puncture site to facilitate hemostasis via endogenous coagulation mechanisms, with manual compression typically requiring 20–30 minutes of applied pressure followed by 6 hours of bed rest, whereas mechanical compression necessitates 2–4

hours of bed rest[58]. However, these methods may result in complications such as pain, skin damage, vascular narrowing, and thrombosis[59]. Vascular closure devices, including Angio-Seal®, Perclose®, and StarClose®, achieve hemostasis by occluding the puncture site with biomaterials or suture-like structure, often reducing the time to hemostasis to 5–10 minutes and bed rest to 1–2 hours[12].

Given that WAP demonstrated the capability to arrest bleeding in a large animal heart within 30 seconds, we hypothesized that WAP might function as an efficient vascular closure device, further minimizing hemostasis time. To validate the vascular closure capacity of WAP, we firstly tested it on a massive bleeding large animal model during open surgery. Specifically, a 20F sheath puncture was created in the porcine abdominal aorta to induce severe arterial bleeding. Upon application, WAP achieved complete hemostasis within 1 minute, effectively sealing the vascular injury and preventing further blood loss (Figure 5a and Supplementary movie 7). To better replicate clinical scenarios of vascular closure, where transfemoral artery punctures are common, we punctured the femoral artery of a pig with a 14F sheath, applied WAP to achieve hemostasis, and subsequently assessed femoral artery blood flow and vascular wound healing following hemostasis. Given the substantial vascular trauma caused by the relatively large diameter of a 14F sheath, our experimental setup encountered considerable bleeding challenges. Even after compressing the proximal end before sheath removal, a significant amount of blood continued to seep from the wound, creating a blurred field of vision and considerable difficulty in achieving hemostasis due to both the volume of blood loss and the vascular pressure at the injury site. WAP was rapidly applied in proximity to the wound site, followed by gentle compression for a duration of 15 seconds, with any residual blood subsequently cleared using sterile medical gauze. A three-minute observation of the wound post-application revealed a uniformly smooth and dry surface, with no signs of blood seepage or hematoma (Figure 5b and supplementary movie 8).

Color Doppler imaging exhibits a strong capability to visualize various states of blood flow, allowing for the detailed assessment of flow pathways and directions. Consequently, we performed Doppler imaging of the femoral artery two weeks post-operation. At this time, the pig was in good condition. The two-dimensional image reveals a clear structure of the femoral arterial wall, with a mildly hyperechoic band-like intimal echo and anechoic blood flow within the lumen. The forward blood flow, displayed in red, shows a uniform laminar flow without any thromboembolic signals (Figure 5c). A low-echo area is observed above the vessel wall, which is likely the WAP. The sharp boundary between the WAP and the vessel wall suggests that WAP occlusion did not interfere with vascular healing, as no pseudoaneurysms were detected. The Doppler blood flow spectral waveform of the femoral artery aligns with laminar flow, presenting a narrowband spectrum. We also observed that in the Doppler contrast image, the reverse blood flow (in blue, Figure 5d), likely from a branch of the femoral artery, also displays a laminar flow pattern, without any signs of embolism or aneurysm. These results indicate successful healing of the femoral artery following WAP occlusion.

These findings from open surgery model confirmed the exceptional rapid closure capability of WAP. Combined

with a suitable delivery accessory, it holds significant potential as an ideal transapical closure device or vascular closure device for hemostasis following puncture with large-sized sheath.

Repair outcome of femoral artery following application of WAP

The tissue samples were collected at two- and four-weeks post-surgery for histological examination, including Hematoxylin and Eosin (HE) staining and immunohistochemical analysis to assess the healing process of the femoral artery and the tissue regeneration at the wound site through macrophage distribution. Similar to normal arteries, the healed femoral artery exhibited a well-preserved three-layer structure, consisting of the intima, media, and adventitia. The artery displayed typical characteristics of a large vessel, with a relatively thick medial layer composed primarily of circularly arranged smooth muscle fibers, with a minor presence of elastic fibers and collagenous connective tissue. No abnormal embolism or false aneurysm was observed in the vessel wall. In the two-week samples, the arterial defect was clearly visible but had been fully sealed. By four weeks, the artery showed further healing despite residual WAP that was still present and did not completely degrade (Figure 6a). Due to the open surgical approach used for femoral artery puncture, notable fibrotic tissue formation was observed surrounding the artery during the healing of the adjacent skeletal muscle, yet this did not interfere with the artery's healing process. Notably, The degradation of the material after arterial puncture was faster than that observed in subcutaneous implantation. This difference is likely due to two factors: the arterial material underwent in situ water-triggered crosslinking, which was less complete than the pre-formed hydrogel used subcutaneously, and the arterial site provided greater exposure to blood and degradative enzymes compared with the relatively stable subcutaneous environment.

The process of tissue healing and regeneration involves the active participation of a large number of inflammatory cells, with the balance between M1 and M2 macrophages playing a critical role in determining the quality and efficiency of tissue repair[60]. Immunohistochemical staining was performed on the vascular injury sites and material implantation sites at both two- and four-weeks post-surgery (Figure 6b-e). At two weeks post-injury, M1 macrophages expressing the iNOS antigen were more abundant than M2 macrophages expressing CD206, indicating that the tissue was in an acute inflammatory phase induced by both surgical trauma and material implantation (Figure 6b–c). By four weeks, the proportion of M1 macrophages had declined (Figure 6d). At the artery injury site, M2 macrophages outnumbered M1, suggesting a transition from acute inflammation to the repair phase. In contrast, at the WAP implantation site, M1 expression remained slightly higher than M2, although the difference was not statistically significant (Figure 6e). This persistent M1 activity may be associated with a foreign body response triggered by material swelling. Nevertheless, this did not hinder wound healing. A comparative analysis of temporal changes in macrophage polarization between the artery injury site and the WAP implantation site further demonstrated that inflammatory responses at the artery injury site had markedly subsided by week four (Supplementary Figure 14a). Around the implanted material, M1 macrophages gradually decreased while M2 macrophages increased, indicating ongoing resolution of the foreign body response as the

material undergoes resorption (Supplementary Figure 14b). Collectively, these findings suggest that WAP supports vascular tissue healing and does not interfere with subsequent repair and regeneration processes.

In this study, we developed a water-activated adhesive patch (WAP) for in vivo hemorrhage control, designed specifically for rapid sealing of severe bleeding sites. The WAP integrates a water-activated adhesive layer with a gelatin sponge, leveraging a composite membrane structure that enhances the hydrogel's mechanical properties while allowing straightforward activation of the adhesive layer in aqueous environments. Using FDA-approved biodegradable PEG derivatives for the adhesive material, our patch demonstrated great biosafety in both *in vitro* and *in vivo* settings. Although the material system has been widely applied in solution form, our strategy enables a distinct patch form of PEG-based adhesive material with superb sealing capacity. Our water-activated adhesion mechanism capitalizes on wet, dynamic tissue as a requisite for bonding, forming an interpenetrating molecular network between the *in situ* crosslinked PEG hydrogel and the tissue ECM. This interaction enabled burst pressures exceeding 300 mm Hg, allowing the WAP to effectively achieve rapid hemostasis in models of severe femoral artery and cardiac apex puncture bleeding. Our findings suggest that the WAP holds promise for clinical translation, offering a potential hemostatic solution for acute traumatic bleeding. The results from the application of WAP following simulated puncture in open surgery effectively demonstrate its safety and efficacy as a potential vascular closure device. Our ongoing efforts focus on designing a customized delivery accessory to complement WAP, aiming to develop an off-the-shelf vascular closure device tailored specifically for puncture procedures involving large-sized sheaths.

Methods

Ethical approval

This research complies with all relevant ethical regulations. Rat and rabbit experiments were conducted in accordance with the guidelines approved by the Zhejiang University Ethics Committee (ZJU20240422). Porcine experiments were approved by The Laboratory Animal Welfare and Ethics Committee of Hangzhou Lifu-Tai biotechnology (IACUC- 20240909-01, IACUC-20250718-03). Only male animals were used in this study. The hemostatic efficacy and in vivo degradation behavior of the materials are primarily determined by their intrinsic physicochemical properties and are minimally affected by sex. The use of male animals also avoided potential physiological variations associated with the estrous cycle, thereby reducing biological variability and improving data consistency.

Preparation and optimization of adhesive layer

PEGDA-1000 (Sinopeg Biotech, China) and 4-arm-PEG-AA (Sinopeg Biotech, China) with different molecular weights were weighed in varying mass ratios and mixed together. The mixture was then placed into a 2 mL syringe and heated in an oven at 65°C for 1 hour until the PEG derivatives melted completely. In another syringe, a mixture of ferrous glucose powder and potassium persulfate powder was prepared. The two syringes were

quickly mixed together at 65°C. The adhesive layer was obtained by injecting the mixture into a polytetrafluoroethylene (PTFE) mold and allowing it to cool and solidify at room temperature. Next, the powdered adhesive layer was obtained by grinding it with a ball mill (50Hz, Shanghai Jingxin) for 1 minute. Adhesive powders with varying molecular weights of 4-arm-PEG-AA, molar ratios of PEGDA-1000 and 4-arm-PEG-AA, and molar ratios of double bonds and redox systems were prepared. The optimal adhesive layer formulation was determined by testing adhesive formation time, integrity of adhesive formation under blood, adhesive properties under water, adhesive properties under blood, and other relevant factors.

Preparation of WAP

The formulation was prepared according to screening results. A mixture of 300 mg PEGDA-1000 and 100 mg 4-arm-PEG-AA (20,000 Da) was heated in an oven at 65°C for 1 hour until the PEG derivatives were completely melted. Another 17.8 mg of ferrous glucose (Macklin, China) powder and 9.5 mg of potassium persulfate (Macklin, China) powder were weighed in another syringe at a molar ratio of PEG derivative-terminated methacrylic acid molecules to ferrous glucose (Fe^{2+}) to potassium persulfate (KPS) = 10:1:1. The two syringes were quickly mixed together at 65°C, resulting in a total mixture volume of approximately 1 mL. The molten mixture was coated on the surface of the Absorbable Gelatin Sponge (Nanjing Jinling Pharmaceutical Factory) at a ratio of 0.25 mL/cm^2 at 65°C. The mixture was then allowed to cool and solidify at room temperature to obtain the final WAP. The prepared WAP was vacuum-sealed and dried for storage. The encapsulated WAPs were sterilized with γ-ray radiation (20 kGy) to obtain sterile WAPs.

Examination of gel formation time of the adherent layer

The polymer mixture solution was prepared by dissolving PEGDA and 4-arm-PEG-AA in a PBS solution. Additionally, the oxidant and reducing agent solution were prepared separately. The reducing agent solution was added to the polymer solution in varying ratios and mixed thoroughly. The oxidant solution was then quickly added to the mixture. Gel formation was monitored and recorded by video, and the gelation time was determined from the recordings.

Examination of the integrity of the gel formation under blood

A 10 mm diameter disc sample was created from the adhesive powder using a mould. The porcine muscle was prepared and submerged in porcine blood. The disc sample was then pressed onto the surface of the muscle in the blood for 15 seconds. The integrity of the hydrogel formed on the tissue surface was assessed after washing the surface thoroughly with PBS.

Adhesive properties of adhesive layer

The adhesion of the material was tested using lap-shear test and 180° peeling test. A universal mechanical tester (MTS Criterion Model 41) with a displacement rate of 10 mm/min was used to record the force and displacement.

For lap shear test, shear strength = F/A, where F is the maximum shear force and A is the adhesion area. For 180° peeling test, interfacial toughness = 2F/d, where F is the plateau tensile force and d is the adhesive width. Data were collected with MTS software TestSuite TW version 4.1.

Wet-surface tissue adhesion properties of adhesive layer: Dry casings were first pasted on one end of the slide, while the other end was kept for mechanical clamping. The slides were then soaked in PBS for 3 minutes to soften the casings, wiped dry, and set aside. Next, the dried adhesive powder was spread on the surface of one of the wiped-dry casings, and the other casing was quickly covered with the surface of the casing with adhesive powder and pressed for 15 seconds. Lap shear tests were performed after the specimen was soaked 2 minutes in water.

Tissue adhesion properties of adhesive layer under blood: Prepare multiple 2 × 0.5 cm muscle samples. Spread the adhesive powder on the end of a piece of muscle tissue with an area of 0.5×0.5 cm. Another piece of muscle tissue was immersed in pig blood. Quickly press one piece of water triggered adhesive powder under the blood to the end of the other for 15 seconds. The surface of the sample after adhesion was cleaned with PBS and then the lap shear test was carried out.

Characterization of the integration of WAP with the tissue

The prepared WAP was pressed on the surface of PBS infiltrated rabbit skeletal muscle isolated tissue for about 30 seconds. The samples were frozen at -80 ℃ for 12 hours and then lyophilized for 48 hours. The samples were broken longitudinally and observed by scanning emission electron microscopy (SEM, FEI, SIRION-100). The micromorphology of the interface between the gelatin sponge layer and the self-adhesive matrix layer, and the interface between the self-adhesive matrix layer and the ECM on the muscle surface in WAP was assessed.

Adhesion and closure of organ by WAP *in vitro*

Porcine visceral organs were used to simulate various types of soft tissue trauma, which was treated with WAP to evaluate the effectiveness of trauma closure.

Closure of Aortic: One end of the porcine aorta was connected to a simulated body fluid and peristaltic pump via a syringe and silicone tubing with a manometer attached. The other end was clamped with hemostats to maintain pressure. After the entire system was filled with fluid, a 5 mm puncture wound was made in the aorta. The wound model was confirmed by squeezing the blood vessel and observing the outflow of fluid. The prepared WAP was pressed onto the aortic tissue for 15 seconds. After sealing, the peristaltic pump was turned on, at which point pressure was increased throughout the system, and a manometer reading was taken to check the effectiveness of the WAP seal and the maximum blood pressure it can withstand.

Closure of stomach: First, completely fill the intact stomach tissue with water. A 5 mm puncture wound was made in the stomach to ensure that the internal water pressure was sufficient to eject a visible jet of water from

the defect. The prepared WAP was pressed onto the stomach tissue for 15 seconds. After sealing, observe if the water flow continues. The gelatin sponge backing of the WAP was then peeled off to check the adhesion of the adhesive layer.

Closure of lung: The syringe was attached to the lung tissue trachea. The lung tissue was placed in simulated body fluid and exhaled fluid was simulated by pushing and pulling the syringe. A 5 mm puncture wound was made in the lung lobe and the prepared WAP was pressed onto the moist lung tissue for 15 seconds. After sealing, the tissue was again immersed in simulated body fluid to observe the success of the seal.

Burst pressure test

Clean casings were cut into 4 × 4 cm sizes and fixed to the test device, which was connected to the manometer. A 2 mm diameter hole was made in the center of the small intestine, and water triggered adhesive powder or WAP with gelatin sponge back film was pressed on the wet surface of the small intestine for 15 seconds to seal the wound. Constant pressure was applied to the defect site through a controlled flow rate (7 mL/min) of the syringe pump, and the pressure gauge reading was recorded. The maximum reading of the pressure gauge before the adhesive rupture was taken as the burst pressure.

***In vitro* degradation of WAP**

WAP samples were accurately weighed and immersed in simulated body fluid (SBF) at 37 °C for up to 28 days. At predetermined time points, samples were carefully removed, lightly blotted to remove surface liquid, and weighed to determine the swollen mass. The swelling ratio was calculated using the following formula:

$$\text{Mass remaining (\%)} = W_0/(W_1-W_0)\times 100\%$$

where W_0 is the initial weight of the sample and W_1 is the weight at each time point. Each measurement was performed in four duplicate, and results were reported as mean ± standard deviation.

***In vitro* cell cytotoxicity assay**

According to ISO10993-5, biological evaluation criteria for medical devices, *in vitro* cytotoxicity of WAP was evaluated by extraction method. To obtain the extract of the experimental group, 2 g of irradiated sterilized WAP was soaked in 20 mL of medium for 24 hours. L929 cells (mouse fibroblasts, Cell Bank of Chinese Academy of Sciences) were inoculated into 96-well plates at 1×10^4 per well, and cultured until the cell fusion reached 90% (n = 5). The cells were cultured for 24, 48, and 96 hours after replacing the complete medium with material extract. Cytotoxicity was detected using the cell counting kit-8 (CCK-8). At each time point, the medium was replaced with DMEM medium containing 10% (v/v) CCK-8 agent. After incubation for 4 hours, the absorbance values were measured at 450 nm using SynergyMx M5 (iD5, Molecular Devices, USA). Data were collected with SoftMax Pro 7.

Cell viability = $A/A_0 \times 100\%$, where A represents the absorbance of the extract group and A_0 represents the absorbance of the normal medium treatment group.

***In vivo* Biodegradability and biocompatibility of WAP**

The animals were operated on in accordance with the guidelines approved by the Zhejiang University Ethics Committee (ZJU20240422). Male rats (Sprague-Dawley, 200-250 g, n=18) were used for the *in vivo* biodegradability and biocompatibility studies. Animals were anesthetized with 2% isoflurane delivered in oxygen via a nose cone throughout the procedure. A 1 cm incision was made in the mediodorsal skin and a lateral subcutaneous pocket was prepared. Under sterile conditions, 18 samples of WAP (10 mm discs) were implanted.

***In vivo* degradation testing**: The rats were euthanized at 7, 14, 28, 56, and 84 days. Samples of the implanted areas were collected to observe the subcutaneous morphology of WAP (n = 3). The tissue and fascia surrounding the sample were removed, and the WAP hydrogel was weighed to draw degradation curves for degradability assessment.

***In vivo* biocompatibility testing**: Rats were euthanized and samples of the implanted areas were harvested at 7, 14, 28, 56 and 84 days (n = 3). The collected samples were fixed in 10% formalin for three days, dehydrated in graded alcohol, and embedded in paraffin for histological evaluation. The sections were stained with hematoxylin and eosin (H&E) for morphological evaluation and to assess inflammatory infiltrate.

Hemostasis and wound closure effect of WAP *in vivo*

Rabbit experiments were conducted in accordance with the guidelines approved by the Zhejiang University Ethics Committee (ZJU20240422). Porcine experiments were approved by The Laboratory Animal Welfare and Ethics Committee of Hangzhou Lifu-Tai biotechnology (IACUC- 20240909-01, IACUC-20250718-03).

Hemostasis of femoral artery hemorrhage in rabbits: Male New Zealand White rabbits (approximately 3 kg, n = 3) were used as a model for arterial hemorrhage hemostasis. After anesthesia with 3% pentobarbital administered via the auricular vein, the femoral artery was incised with a scalpel without separating the surrounding muscle, simulating acute injuries such as battlefield trauma. The hemostatic effect of the WAP was then assessed by applying the patch to the incision for 30 seconds.

Hemostasis of hemorrhages in the porcine heart: Male Bama mini pigs (approximately 25 kg, n=3) was administered Telazol (5 mg/kg, i.m.) and propofol (1.5 mL/kg, i.m.) until achieving complete sedation. Subsequently, oral double-lumen tracheal intubation was performed, followed by inhalational anesthesia using isoflurane, and mechanical ventilation was initiated at a rate of 15 breaths per minute with a tidal volume of 10 mL/kg. The pig was positioned supinely, and the sternum was incised to expose the heart. In order to assess the hemostatic efficacy of WAP on cardiac injuries, an approximately 2 cm long puncture wound was created on the heart using an 18-gauge scalpel (n = 3). Following this, the wounds and adjacent tissue were promptly subjected

to pressure using sterile WAP to arrest bleeding for a duration of 60 seconds. Subsequent observation and documentation of the hemostatic process were conducted.

Hemostasis after abdominal aortic bleeding in Bama mini pigs: Male Bama mini pigs (approximately 25 kg, n=3) were anesthetized as described above. Following anesthesia, a midline abdominal incision of approximately 10–12 cm was made, and the abdominal aorta was carefully exposed by blunt dissection. After isolating a segment of the abdominal aorta, a puncture was generated using 20F catheter sheath on the vessel wall, resulting in immediate high-pressure arterial bleeding. To evaluate the hemostatic performance of WAP, the patch was immediately applied over the bleeding site and pressed for 60 s to ensure adhesion. Excess blood around the patch was removed with sterile gauze, and the hemostatic outcome was assessed visually. Vital signs, including heart rate, blood pressure, and oxygen saturation, were continuously monitored using a multifunctional monitor throughout the procedure. After confirmation of hemostasis, the abdominal wall and skin were sutured in layers, and the surgical site was sterilized with povidone-iodine. Postoperatively, animals were monitored until full recovery from anesthesia and received intramuscular potassium penicillin (20,000 units/kg) daily for three days to prevent infection.

Hemostasis after femoral artery puncture in Bama mini pigs: Male Bama mini pigs (approximately 30 kg, n=3) was sedated following the aforementioned procedure. Following the anesthesia, the skin of the Bama mini-pigs near the groin was prepared and sterilized with povidone-iodine. The femoral artery is visualized by incising the skin for approximately 5 cm and separating the perivascular tissue with a vascular clamp. A puncture needle was inserted into the femoral artery at an angle of 30-45 degrees until brightly colored arterial blood gushes from the needle to ensure that it enters the correct vascular site. The guidewire is threaded through the end of the puncture needle and advanced to the desired depth. Afterwards, a 14F catheter sheath with a dilator tube was threaded through the end of the guidewire following the removal of puncture needle. Immediately after the catheter was delivered into the femoral artery, the guidewire and dilator tube were removed. By far, a puncture on femoral artery had been successfully established. To evaluate the potential of WAP as a vascular closure device, the catheter is first removed, followed by the introducer sheath. WAP is applied immediately on the puncture site to stop bleeding when the introducer is withdrawn. After pressing WAP for 30 s, sterile gauze was used to clean the excess blood to observe whether the hemostasis was complete. And the vital signs of the Bama mini pigs were detected with a multifunctional monitor. Last, the muscle and skin tissues were sutured and the wound was sterilized with povidone-iodine. Bama mini-pigs were observed for normal awakening status after anesthesia, and potassium penicillin (20,000 units/kg) was injected intramuscularly daily for three days after surgery to prevent infection.

Electrocardiography and Echocardiography of Pigs

For cardiac monitoring, Male Bama mini pigs (approximately 25 kg, n=4) were anesthetized using standard protocols to minimize stress and movement. Electrocardiograms (ECG) were recorded using a multi-lead

veterinary ECG system (Mindray Technology, China). Electrodes were placed according to standard limb and chest positions, and recordings were acquired at a sampling rate sufficient to capture cardiac electrical activity. ECGs were collected at baseline (pre-surgery) and at designated postoperative time points.

Echocardiography was performed using a high-resolution veterinary ultrasound system equipped with a phased-array transducer suitable for porcine cardiac imaging (Mindray Technology, China). Pigs were placed in a supine or lateral recumbent position. Two-dimensional (2D) and M-mode images were obtained from standard parasternal and apical views to assess cardiac structure and function. Parameters including left ventricular end-diastolic volume (EDV), left ventricular internal diameter at diastole (LVIDd), stroke volume (SV), ejection fraction (EF), and end-systolic volume (ESV) were measured. Images and cine loops were recorded for offline analysis.

Color Doppler ultrasound (CDU) testing

CDU testing was performed 2 weeks after the operation on a RFLSI III Laser speckle blood flow imaging system (RWD Life Science, China). The pig was placed in a supine position to ensure blood return and maintain a certain degree of femoral artery filling during the operation of color Doppler flow imaging. The patency, lumen diameters, and flow velocities were evaluated using the color mode and pulse wave mode. The pulse Doppler frequency (Fq) was 6.3 MHz and the pulse repetition frequency (PRF) was 5.4 kHz.

Histology and IHC of CD206 and iNOS

After CDU testing, Bama mini-pigs were euthanized, and samples were harvested at 2 and 4 weeks. The collected femoral arteries were fixed in 10% formalin for 3 days, sequentially dehydrated in graded alcohol, and embedded in paraffin for histological evaluation. The sections were stained with H&E for morphological evaluation and to assess inflammatory infiltrate. To further investigate the specific contents of CD68 and CD206, sections were assessed through IHC staining. The CD206 antibody (1:1000 dilution, NBP1-90020, Novus) and iNOS antibody (1:100 dilution, NB300-605, Novus) were used with staining according to the manufacturer's protocol. ImageJ was used with thresholding tool to calculate the positive area.

Statistical analysis

All the experiments were repeated for at least three times The data were expressed as mean ± standard deviation. One-way analysis of variance (ANOVA) was used to assess the differences between groups.

Data Availability

All relevant data are available within the article and Supplementary information. Source data are provided with this paper. All data underlying this study are available from the corresponding author upon request.

References

1. Slawin, J.*, et al.* Radial artery occlusion after percutaneous coronary interventions - an underestimated issue. *Postepy Kardiol Interwencyjnej* **9**, 353-361 (2013).
2. Chen, I.M., Lee, T.-H., Chen, P.-L., Shih, C.-C. & Chang, H.-H. Factors in ProGlide® Vascular Closure Failure in Sheath Arteriotomies Greater than 16 French. *European Journal of Vascular and Endovascular Surgery* **58**, 615-622 (2019).
3. Hu, G.*, et al.* Predictors and treatments of Proglide-related complications in percutaneous endovascular aortic repair. *PLoS One* **10**, e0123739 (2015).
4. Georgiadis, G.S.*, et al.* A meta-analysis of outcome after percutaneous endovascular aortic aneurysm repair using different size sheaths or endograft delivery systems. *J Endovasc Ther* **18**, 445-459 (2011).
5. Manunga, J.M.*, et al.* Femoral artery calcification as a determinant of success for percutaneous access for endovascular abdominal aortic aneurysm repair. *J Vasc Surg* **58**, 1208-1212 (2013).
6. Sekhar, A.*, et al.* Femoral arterial closure using ProGlide(R) is more efficacious and cost-effective when ambulating early following cardiac catheterization. *Int J Cardiol Heart Vasc* **13**, 6-13 (2016).
7. Walther, T., Arsalan, M., Kim, W. & Kempfert, J. TAVI: transapical--what else? *EuroIntervention* **9 Suppl**, S19-24 (2013).
8. Dudiy, Y.*, et al.* Percutaneous transapical access: current status. *EuroIntervention* **10 Suppl U**, U84-89 (2014).
9. Ziegelmueller, J.A., Lange, R. & Bleiziffer, S. Access and closure of the left ventricular apex: state of play. *J Thorac Dis* **7**, 1548-1555 (2015).
10. Ferrari, E., Pozzoli, A., Maisano, F. & von Segesser, L.K. Apical closure device for full-percutaneous transapical structural and valve procedures with large-sized introducer sheaths: The final preclinical study. *J Card Surg* **37**, 1877-1884 (2022).
11. Jaffer, I.H., Fredenburgh, J.C., Hirsh, J. & Weitz, J.I. Medical device-induced thrombosis: what causes it and how can we prevent it? *J Thromb Haemost* **13 Suppl 1**, S72-81 (2015).
12. Noori, V.J. & Eldrup-Jorgensen, J. A systematic review of vascular closure devices for femoral artery puncture sites. *J Vasc Surg* **68**, 887-899 (2018).
13. Sharma, R., Vamanan, K. & Gupta, K. Treatment of Angio-Seal(R) Vascular Closure Device-Induced Acute Femoral Artery Occlusion with SilverHawk(R) Directional Atherectomy. *Cureus* **8**, e910 (2016).
14. Addepalli, A.*, et al.* Risk of Ipsilateral Deep Vein Thrombosis After Use of AngioSeal Closure Device in Aneurysmal Subarachnoid Hemorrhage Patients. *World Neurosurg* **134**, e162-e165 (2020).
15. Megaly, M.*, et al.* Complications of the MANTA Closure Device: Insights From MAUDE Database. *Cardiovasc Revasc Med* **34**, 75-79 (2022).
16. Cianci, C.*, et al.* Critical lower limb ischemia from an embolized Angio-Seal closure device. *Proc (Bayl Univ Med Cent)* **26**, 398-400 (2013).
17. Ben-Dor, I.*, et al.* MynxGrip(R) vascular closure device versus manual compression for hemostasis of percutaneous transfemoral venous access closure: Results from a prospective multicenter randomized study. *Cardiovasc Revasc Med* **19**, 418-422 (2018).
18. Hackl, G.*, et al.* Exoseal for puncture site closure after antegrade procedures in peripheral arterial disease patients. *Diagn Interv Radiol* **20**, 426-431 (2014).
19. Chansoria, P.*, et al.* Instantly adhesive and ultra-elastic patches for dynamic organ and wound repair. *Nat Commun* **15**, 4720 (2024).

20. Pal, S.*, et al.* Recyclable surgical, consumer, and industrial adhesives of poly(alpha-lipoic acid). *Science* **385**, 877-883 (2024).
21. Wu, S.J.*, et al.* A 3D printable tissue adhesive. *Nature Communications* **15**(2024).
22. Inoue, A., Yuk, H., Lu, B. & Zhao, X. Strong adhesion of wet conducting polymers on diverse substrates. *Science Advances* **6**(2020).
23. Yuen, H.Y., Bei, H.P. & Zhao, X. Underwater and wet adhesion strategies for hydrogels in biomedical applications. *Chemical Engineering Journal* **431**(2022).
24. Wu, J.*, et al.* An off-the-shelf bioadhesive patch for sutureless repair of gastrointestinal defects. *Science Translational Medicine* **14**(2022).
25. Cui, C. & Liu, W. Recent advances in wet adhesives: Adhesion mechanism, design principle and applications. *Progress in Polymer Science* **116**(2021).
26. Cui, C.*, et al.* Water-Triggered Hyperbranched Polymer Universal Adhesives: From Strong Underwater Adhesion to Rapid Sealing Hemostasis. *Adv Mater* **31**, e1905761 (2019).
27. Zheng, S.Y.*, et al.* Water-Triggered Spontaneously Solidified Adhesive: From Instant and Strong Underwater Adhesion to In Situ Signal Transmission. *Advanced Functional Materials* **32**(2022).
28. Su, X.*, et al.* Strong underwater adhesion of injectable hydrogels triggered by diffusion of small molecules. *Mater Horiz* **8**, 2199-2207 (2021).
29. Liu, Y.*, et al.* Synthesis of robust underwater glues from common proteins via unfolding-aggregating strategy. *Nat Commun* **14**, 5145 (2023).
30. Slezak, P.*, et al.* Tissue reactions to polyethylene glycol and glutaraldehyde-based surgical sealants in a rabbit aorta model. *J Biomater Appl* **34**, 1330-1340 (2020).
31. Lewis, K.M., Kuntze, C.E. & Gulle, H. Control of bleeding in surgical procedures: critical appraisal of HEMOPATCH (Sealing Hemostat). *Med Devices (Auckl)* **9**, 1-10 (2016).
32. Slezak, P.*, et al.* Properties of collagen-based hemostatic patch compared to oxidized cellulose-based patch. *J Mater Sci Mater Med* **29**, 71 (2018).
33. Yang, R.*, et al.* Tunable backbone-degradable robust tissue adhesives via in situ radical ring-opening polymerization. *Nat Commun* **14**, 6063 (2023).
34. Yang, J., Bai, R. & Suo, Z. Topological Adhesion of Wet Materials. *Adv Mater* **30**, e1800671 (2018).
35. Ma, Z.*, et al.* Controlled tough bioadhesion mediated by ultrasound. *Science* **377**, 751-755 (2022).
36. Zeng, Z.*, et al.* An in situ forming tissue adhesive based on poly(ethylene glycol)-dimethacrylate and thiolated chitosan through the Michael reaction. *J Mater Chem B* **4**, 5585-5592 (2016).
37. Granskog, V.*, et al.* High-Performance Thiol–Ene Composites Unveil a New Era of Adhesives Suited for Bone Repair. *Advanced Functional Materials* **28**(2018).
38. Kharkar, P.M., Rehmann, M.S., Skeens, K.M., Maverakis, E. & Kloxin, A.M. Thiol-ene click hydrogels for therapeutic delivery. *ACS Biomater Sci Eng* **2**, 165-179 (2016).
39. Robinson, J.W.*, et al.* Probing the molecular design of hyper-branched aryl polyesters towards lubricant applications. *Sci Rep* **6**, 18624 (2016).
40. Anindita, S.N.*, et al.* Tough PEG-only hydrogels with complex 3D structure enabled by digital light processing of "all-PEG" resins. *Aggregate* **4**(2023).
41. Yuk, H.*, et al.* Rapid and coagulation-independent haemostatic sealing by a paste inspired by barnacle glue. *Nat Biomed Eng* **5**, 1131-1142 (2021).

42. Yu, L., *et al.* Sequential-Crosslinking Fibrin Glue for Rapid and Reinforced Hemostasis. *Adv Sci (Weinh)* **11**, e2308171 (2024).
43. Lu, Y., *et al.* Silk Fibroin-Based Tough Hydrogels with Strong Underwater Adhesion for Fast Hemostasis and Wound Sealing. *Biomacromolecules* **24**, 319-331 (2023).
44. Zheng, Y., *et al.* Hemostatic patch with ultra-strengthened mechanical properties for efficient adhesion to wet surfaces. *Biomaterials* **301**, 122240 (2023).
45. Zhang, K., *et al.* Tough Hydrogel Bioadhesives for Sutureless Wound Sealing, Hemostasis and Biointerfaces. *Advanced Functional Materials* **32**(2021).
46. Wu, W., *et al.* Polyurethane-Based Bioglue for the Repair of Arterial Ruptures. *Advanced Functional Materials* (2024).
47. Yuk, H., *et al.* Dry double-sided tape for adhesion of wet tissues and devices. *Nature* **575**, 169-174 (2019).
48. Zhou, J., *et al.* Adhesion properties of catechol-based biodegradable amino acid-based poly(ester urea) copolymers inspired from mussel proteins. *Biomacromolecules* **16**, 266-274 (2015).
49. Wang, L., *et al.* A Novel Double-Crosslinking-Double-Network Design for Injectable Hydrogels with Enhanced Tissue Adhesion and Antibacterial Capability for Wound Treatment. *Advanced Functional Materials* **30**(2019).
50. Ren, H., *et al.* Injectable, self-healing hydrogel adhesives with firm tissue adhesion and on-demand biodegradation for sutureless wound closure. *Science Advances* **9**(2023).
51. Hong, Y., *et al.* A strongly adhesive hemostatic hydrogel for the repair of arterial and heart bleeds. *Nat Commun* **10**, 2060 (2019).
52. Latif, R.K., *et al.* Traumatic hemorrhage and chain of survival. *Scand J Trauma Resusc Emerg Med* **31**, 25 (2023).
53. Alvis, B.D., Brophy, C., Cheung-Flynn, J., Case, M. & Hocking, K. A Porcine Model of Acute Respiratory Failure with a Continuous Infusion of Oleic Acid. *J Vis Exp* (2024).
54. Darya, G., Mohammadi, H., Dehghan, Z., Nakhaei, A. & Derakhshanfar, A. Animal models of hemorrhage, parameters, and development of hemostatic methods. *Lab Anim Res* **41**, 5 (2025).
55. Vora, A.N. & Rao, S.V. Percutaneous or surgical access for transfemoral transcatheter aortic valve implantation. *J Thorac Dis* **10**, S3595-S3598 (2018).
56. Ortiz, D., *et al.* Access site complications after peripheral vascular interventions: incidence, predictors, and outcomes. *Circ Cardiovasc Interv* **7**, 821-828 (2014).
57. Petroglou, D., *et al.* Manual Versus Mechanical Compression of the Radial Artery After Transradial Coronary Angiography: The MEMORY Multicenter Randomized Trial. *JACC Cardiovasc Interv* **11**, 1050-1058 (2018).
58. Maqsood, M.H., *et al.* Optimal Hemostatic Band Duration After Transradial Angiography or Intervention: Insights From a Mixed Treatment Comparison Meta-Analysis of Randomized Trials. *Circ Cardiovasc Interv* **16**, e012781 (2023).
59. Wu, B., Zhang, R., Liang, C., Zhang, C. & Qin, G. Study on the Safety of the New Radial Artery Hemostasis Device. *J Interv Cardiol* **2022**, 2345584 (2022).
60. Chen, S., *et al.* Macrophages in immunoregulation and therapeutics. *Signal Transduct Target Ther* **8**, 207 (2023).

Acknowledgements

This work is supported by the National Key Research and Development Program of China (2023YFE0206700 to H.O.), the National Natural Science Foundation of China (T2121004 to H.O., 92268203 to H.O.), and Key R&D Program of Zhejiang (2024SSYS0028 to H.O.). The authors thank Guizhen Zhu in the Center of Cryo-Electron Microscopy (CCEM), Zhejiang University for her technical assistance on SEM. The authors thank Dr. Zhiyang Yu from Accelerator Center of Zhejiang University for providing support on material processing. The authors thank Ms. Ruochen Yang for her contributions to the graphic illustrations in this manuscript.

Author contributions

Yuxuan Huang, Qiuwen Zhu, and Yuqing Gu: Conceptualization, Data curation, Formal Analysis, Investigation, Methodology, Project administration, Resources, Original draft writing. Rong Wang: Investigation, Methodology, Resources, Original draft writing. Qianqian Zhu: In vivo rabbit and pig experiments. Chang Xie, Qi Jiang, Renjie Liang, and Yi Zhang: In vivo rabbit experiments. Youzhi Cai: Conceptualization, Supervision, In vivo rabbit and pig experiments. Yi Hong: Conceptualization, Supervision, Reviewing and editing draft. Hongwei Ouyang: Conceptualization, Funding acquisition, Resources, Supervision, Reviewing and editing draft. All authors reviewed and approved the submitted manuscript.

Competing interests

The authors declare no competing interests.

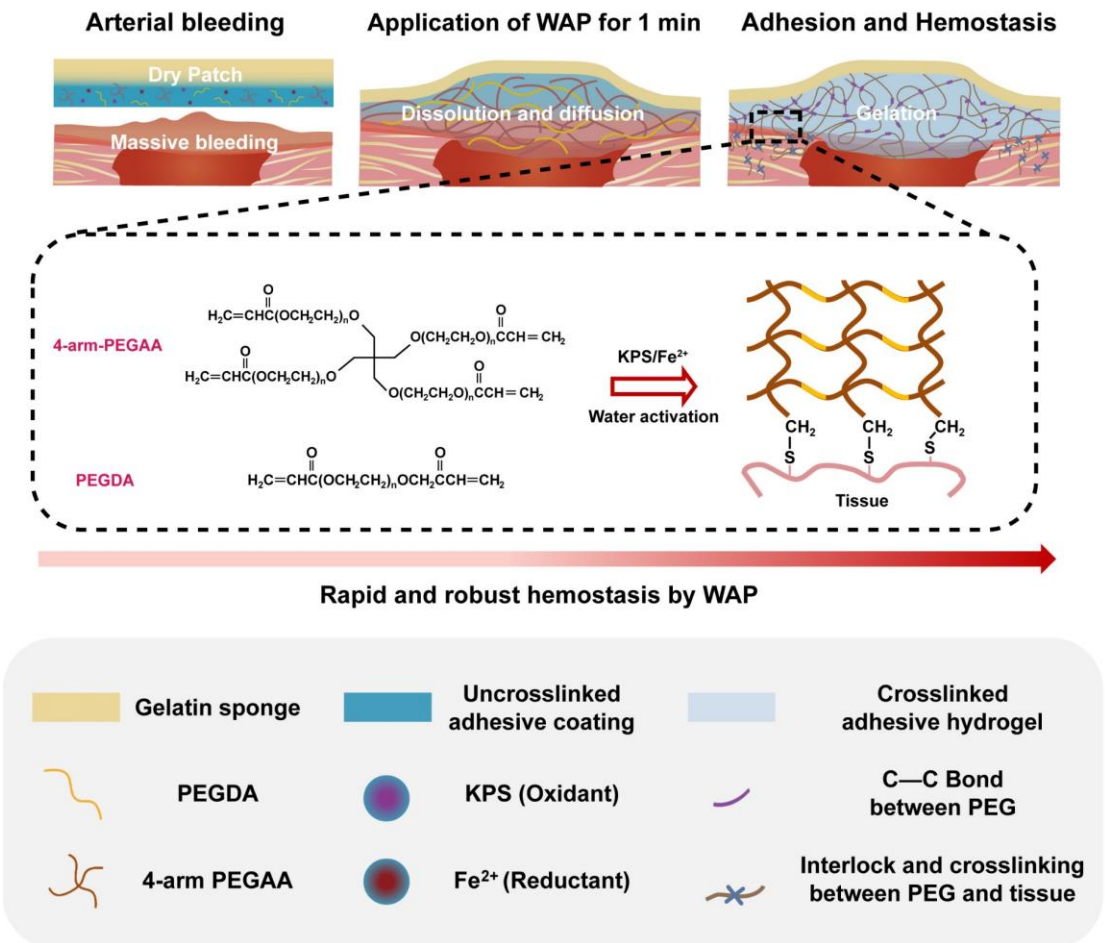

Figure 1. Schematic illustrations of WAP. Upon exposure to Body fluids, the polymer and the oxidant/reductant catalyst dissolve and initiate gelation. The acrylate-modified PEG adheres to tissue through mechanical interlocking and via Michael addition with thiol groups present in the extracellular matrix (ECM). WAP is applied manually by the operator and applying pressure varies depending on the wound site, bleeding severity, and patient condition. As such, it is not feasible to define or standardize an absolute pressure value. KPS: potassium persulfate.

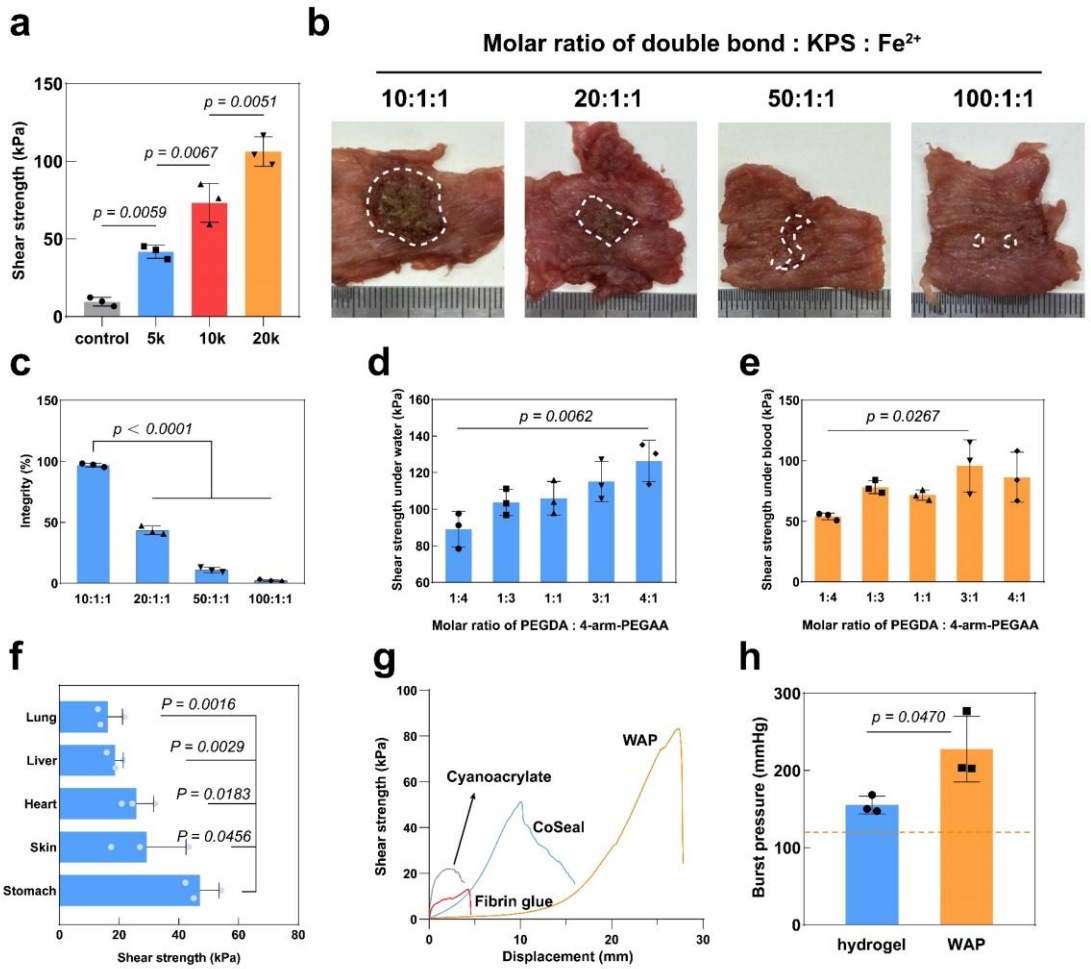

Figure 2. WAP exhibits strong wet adhesive properties following optimization of its component ratio. a. Shear strength of adhesive powder fabricated with PEGDA-1000 and 4-arm PEGAA with various molecular weights. **b.** Digital photos showing the integrity of hydrogel formed with different ratio of double bond and redox system. **c.** Quantitative analysis of integrity in (**b**). **d-e.** Shear strength of adhesive powder with various ratio of PEGDA-1000 and 4-arm PEGAA, using (**d**) water or (**e**) blood as interface liquid. **f.** Shear strength of adhesive powder on various organs. **g.** Lap shear curve of WAP and various commercial adhesive products. **h.** Burst pressure of WAP with or without adhesive layer. Data are presented as mean±standard error. Exact p-value for multiple comparisons is calculated with one-way ANOVA Tukey's multiple comparisons test. Statistical significance between two groups is calculated with two-tailed Student's t-test. Each group included three independent replicates. KPS: potassium persulfate.

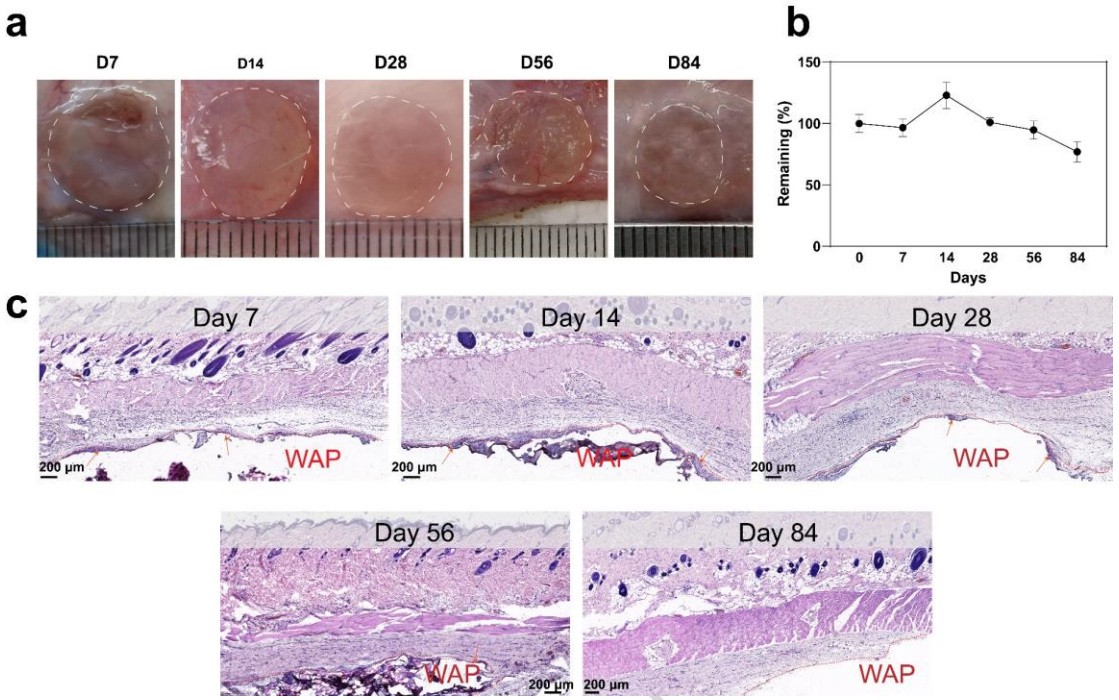

Figure 3. WAP could degrade subcutaneously and exhibit good biocompatibility. a. Digital photos showing the morphological change of WAP following subcutaneous implantation. **b.** Relative change in weight of WAP following subcutaneous implantation. **c.** H&E staining of subcutaneously implanted WAP at different time point. n = 3 rats per time point. Data are presented as mean±standard error. Scale Bar: 200μm.

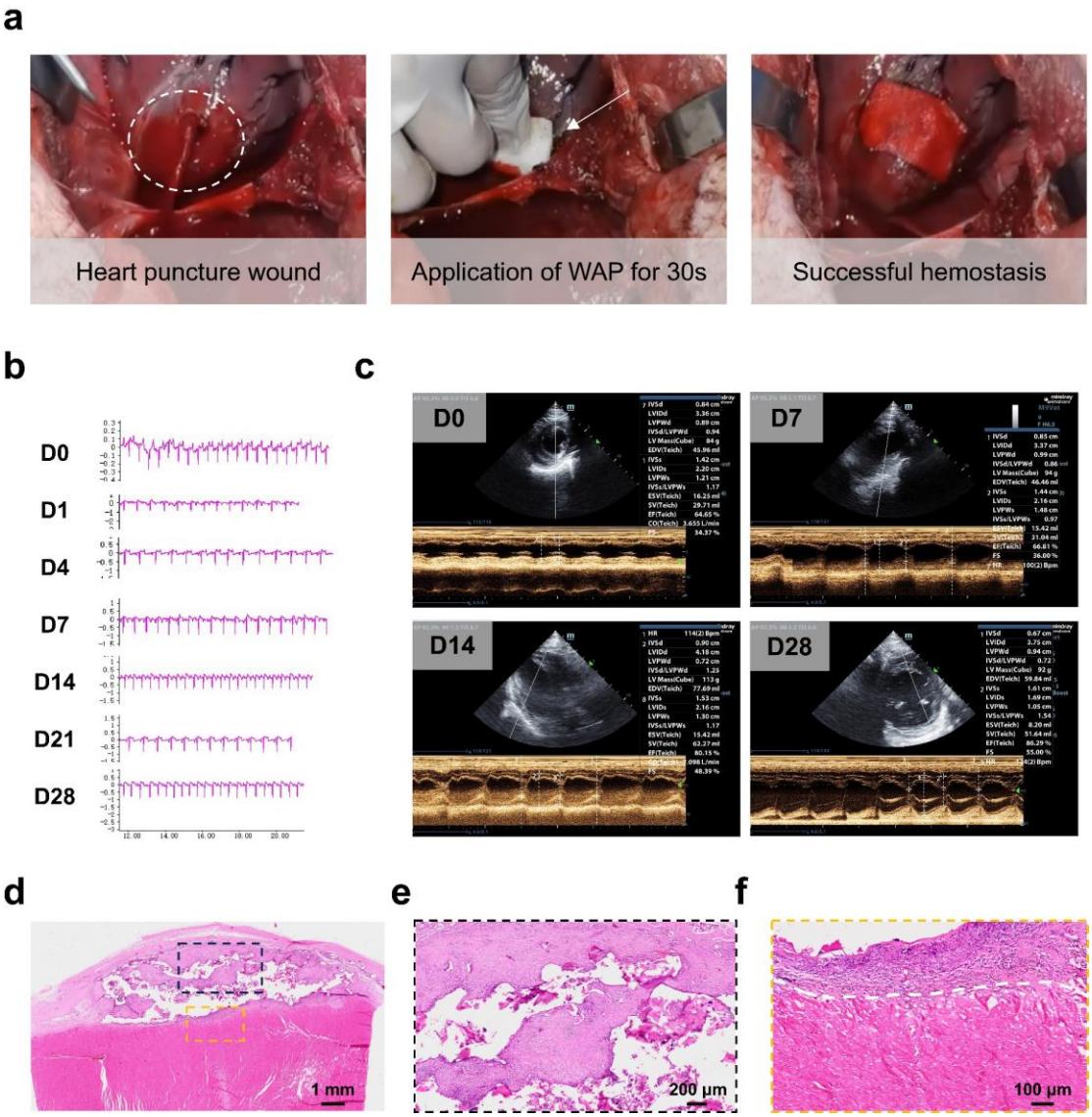

Figure 4. WAP effectively achieves hemostasis following cardiac puncture and facilitates wound repair. a. Digital photos showing the application of WAP on a cardiac apex hemorrhage. **b.** Representative electrocardiograms from pre-operation (D0) to 28 days post-operation. **c.** Representative echocardiographic images from pre-operation (D0) to 28 days post-operation. **d.** H&E staining of the injury site at 28 days post-operation. **e.** H&E staining of remaining WAP and surrounding tissue in (**d**). **f.** H&E staining of the WAP-tissue interface (white dashed line) in (**d**). n = 4 pigs.

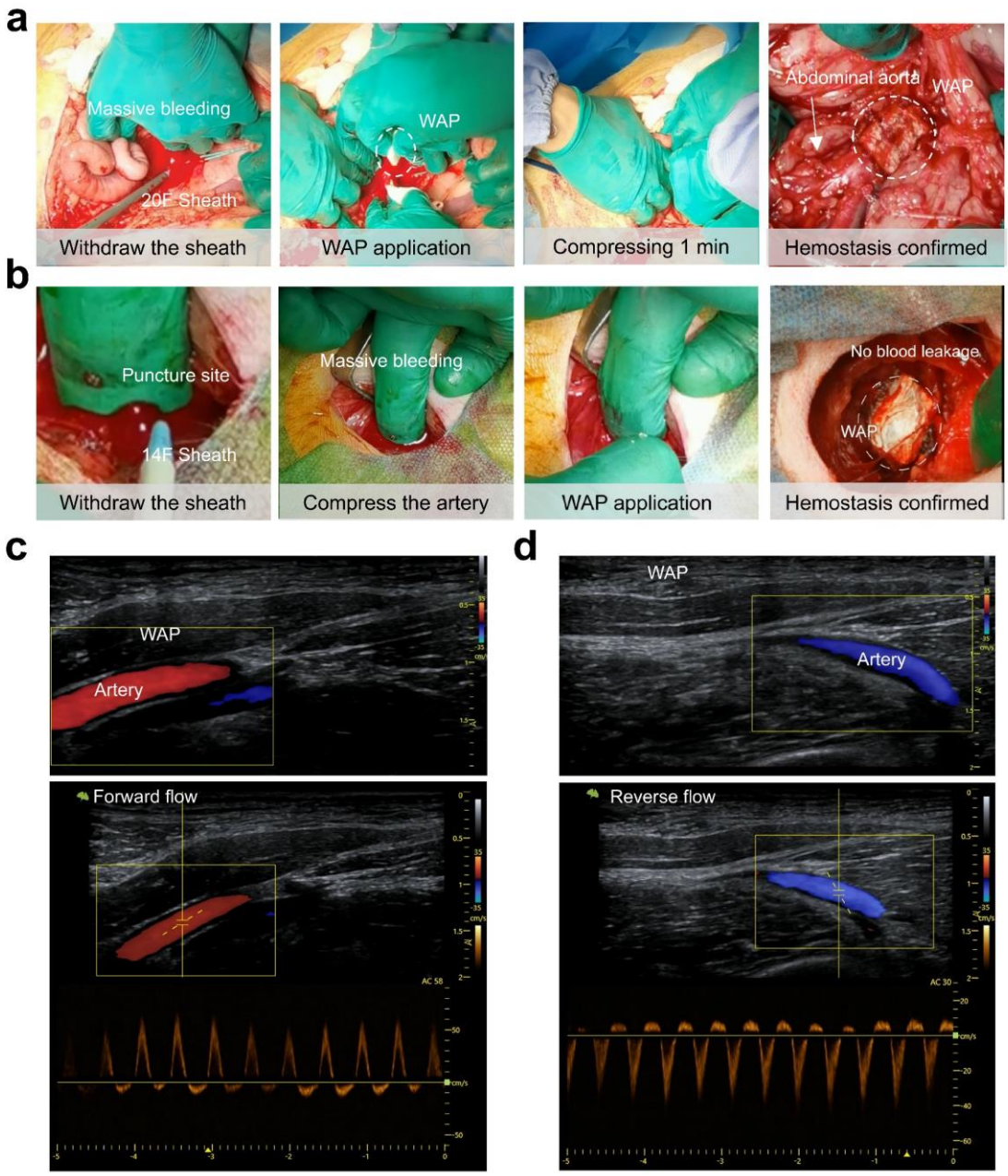

Figure 5. WAP effectively achieves hemostasis following artery puncture and facilitates wound repair. a. Digital photos showing the application of WAP after removal of a 20F puncture sheath from a porcine abdominal aorta. **b.** Digital photos showing the application of WAP after removal of a 14F puncture sheath from a porcine femoral artery. **c-d.** two-dimensional images (top) showing the (**c**) forward-flowing blood and (**d**) reverse-flowing blood through the femoral artery. The corresponding spectral analysis (bottom) showed the velocity and frequency distribution of the blood flow. n = 3 pigs per experiment.

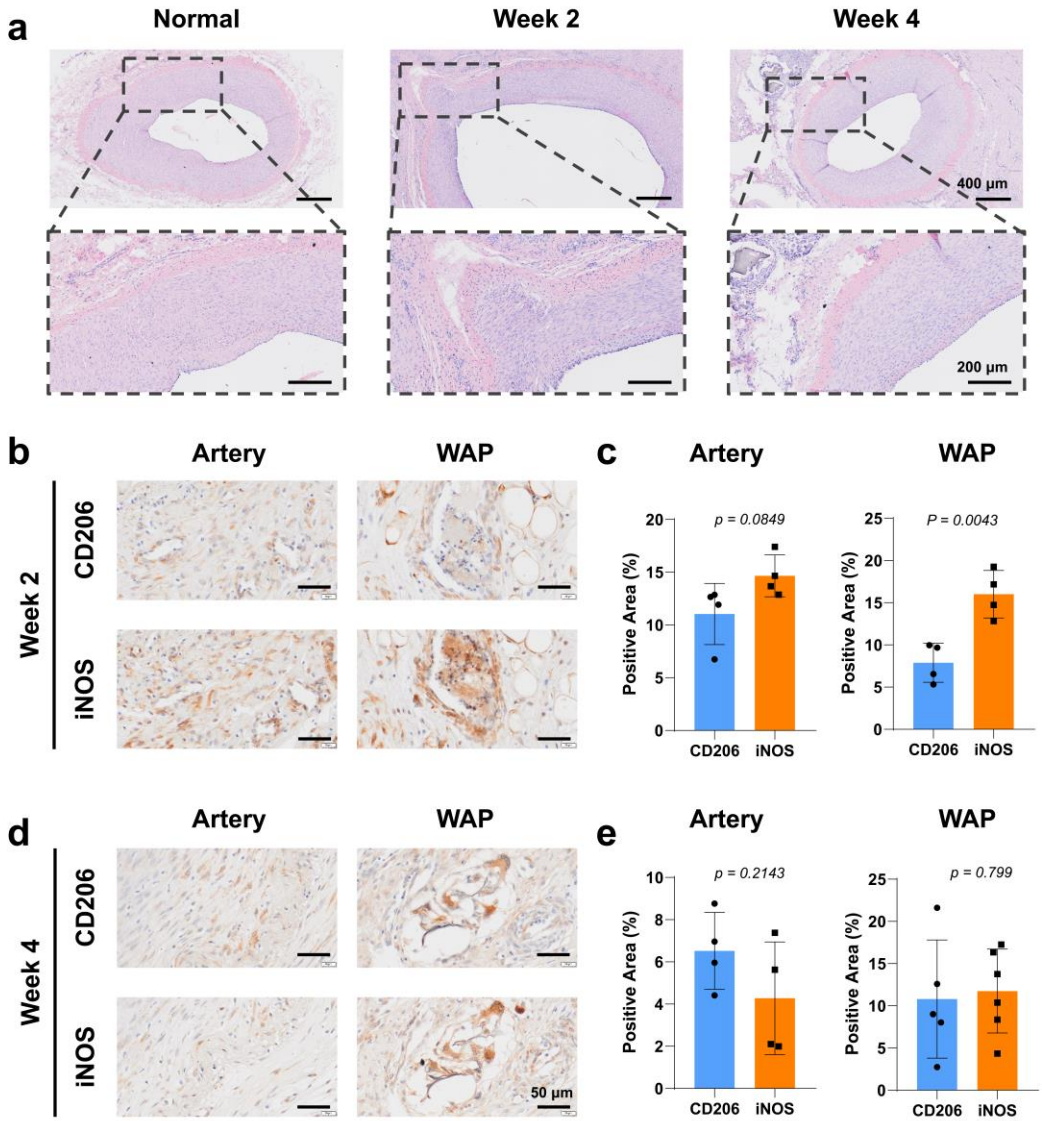

Figure 6. WAP induced moderate inflammation response during the repair process of the porcine femoral artery. a. H&E staining of porcine femoral artery 2 weeks and 4 weeks post-surgery. Normal femoral artery serves as control. **b.** Immunohistochemical (IHC) staining of porcine femoral artery 2 weeks post-surgery. **c.** Quantitative analysis of the IHC staining results in (**b**). **d.** IHC staining of porcine femoral artery 4 weeks post-surgery. **e.** Quantitative analysis of the IHC staining results in (**d**). n = 3 pigs per group and per time point. Data are presented as mean ± standard error. Statistical significance between two groups is calculated with two-tailed Student's t-test.

Sealing of puncture points after interventional surgeries is a vital requirement, but large diameter sheaths and transapical punctures present a significant challenge for wound closure. Here, the authors present a water-activated tissue adhesive patch designed for quick and strong adhesion to blood vessel and heart tissue surfaces after surgery.

Peer Review Information: *Nature Communications* thanks Parth Chansoria, who co-reviewed with Michael Winkelbauer, and the other, anonymous, reviewer(s) for their contribution to the peer review of this work. A peer review file is available.